



# Nonlinear complementarity equations for modeling tire–soil interaction—An incremental Bekker approach

S.G. Mao<sup>a</sup>, Ray P.S. Han<sup>b,\*</sup>

<sup>a</sup>*Mechanical Simulation Technologies, CAE Division, LMS International, Coralville, IA 52241, USA*

<sup>b</sup>*Department of Advanced Materials and Nanotechnology, Peking University, 100871 Beijing, China*

Received 9 September 2005; received in revised form 29 January 2007; accepted 9 July 2007

Available online 20 February 2008

## Abstract

In this work, an accurate computational model for analyzing tire–soil interaction problems is described. In the traditional approach, Bekker equation is written in a global form and a quasi-static analysis is then carried out to iteratively capture the interaction of the tire, which is modeled as a rigid wheel and the soil. The iteration is tedious but required in order to model the nonlinear relationship between soil sinkage and pressure, and the unknown loading/unloading/reloading status of the soil that is dependent on past histories. An incremental form of Bekker model is proposed to overcome some of the difficulties in the traditional approach. The method involves formulating the contact dynamics with a set of complementarity equations. This approach allows the contact forces to be evaluated as part of the solution of the unknown kinematics, and thereby, stay current during an iteration. In contrast, the contact forces in the traditional Bekker method are always be one time-step back. The net result is enhanced computational accuracy and convergency for the proposed incremental Bekker approach. Two examples are solved to demonstrate the effectiveness of the proposed algorithm. Solutions for soil sinkage, drawbar pull, normal pressure, and shear stress for a tire interacting with three types of soil; loose sand, soft soil, and LETE sand are provided and compared with published results. The comparison shows good agreement.

© 2007 Elsevier Ltd. All rights reserved.

## 1. Introduction

One of the key determinants in assessing the performance of off-road vehicles in terms of ride comfort and safety is the dynamics interaction between the tire and the soil. A comprehensive survey of this research area is described in Schmid [1]. The techniques for investigating the tire–soil interaction problem can be broadly grouped into three categories: (a) analytic methods [2], (b) empirical methods [3], and (c) finite element methods [4,5]. In his classic book, Wong [6] provided a good introduction of the first two methods. The third approach is very popular with several finite element models having been proposed. Hiroma et al. [4] investigated stress distributions under a wheel by accounting for the friction and adhesion between the wheel and soil using a viscoelastic finite element soil model. Liu and Wong [5] suggested a finite element-based critical state soil mechanics approach for handling tire–soil interaction. They looked at the tractive

\*Corresponding author. Tel.: +8610 6276 7394.

E-mail address: ray-han@coe.pku.edu.cn (R.P.S. Han).

Nomenclature			
$A_u$	parameter characterizing terrain response to repetitive loading	$k_\phi$	friction soil modulus
$b$	smaller dimension of the tire footprint	$n$	exponent employed in Bekker equation (see Eq. (1))
$b_{tr}$	tire width	$p$	normal pressure
$c$	soil cohesion	$p_u$	peak pressure at the start of the unloading
$c_g$	geometric damping constant	$s$	shear stress
$F_{sd}$	damping force of the tire during unloading or reloading of soil	$s_{max}$	maximum shear stress
$f_i$	friction stress at time $t$	$y_c, z_c$	coordinates of the tire's mass center
$g_i^n$	gap function	$W$	wheel load
$\dot{g}_i^t$	relative tangential velocity	$z$	sinkage
$j$	shear displacement	$z_e$	recoverable or elastic sinkage
$K$	shear deformation modulus	$z_p$	irrecoverable or plastic sinkage
$k_c$	cohesive soil modulus	$z_{u1}, z_{u1}$	peak sinkage at the start of the unloading, limit value (see Eq. (6))
$k_0$	parameter characterizing terrain response to repetitive loading	$\phi$	angle of shearing resistance
$k_u$	terrain stiffness during unloading or reloading	$\eta, \eta_1, \eta_0$	rebound ratio (see Eq. (5)), rebound ratio for $z_{u1}$ , rebound ratio as $z_u \rightarrow 0$

performance of rigid wheels moving on sand. Wulfsohn and Upadhyaya [7] predicted traction and soil compaction using two- and three-dimensional tire–soil contact profiles. To compute the pressure distribution, they used a semi-logarithmic porosity–stress relationship in their soil model. Fassbender et al. [8] and Grahn [9] investigated the vehicle dynamics on soft soil by adopting a dynamic pressure–sinkage relationship that is dependent on the penetration velocity. Through a series of careful experimental measurements, Onafeko and Reece [10] obtained stress distributions on the tire–soil interface.

To accurately capture the effects of tire–soil interaction, it is necessary to properly formulate the model by taking into consideration the coupled and nonlinear problems of deformable tire dynamics, tire–soil contacts, and soil elasto-plastic deformations. A high-fidelity model of the tire–soil contact interaction model can therefore, be complex and computationally challenging. Most of the current analyses are based on a quasi-static equilibrium approach with an assumed slip. These methods can yield meaningful results, particularly, when parametric studies of the performance are required. If a realistically accurate prediction is required, improvements and modifications for these methods are necessary. The popular approach is to resort to using finite element-based models. However, a time integration of the elasto-plastic finite element model of a moving vehicle for its dynamic response can be tedious and expensive. Hence, the Bekker model [6,11] is still widely used to reduce order of complexity in the numerical computations.

In this work, an incremental form of Bekker model is proposed. It leads to a set of nonlinear complementarity equations for characterizing tire–soil interaction. These equations describe the dynamic contacts between the tire and soil with friction, and allow the contact forces of pressures and friction to be solved directly as part of the solution of the unknown tire kinematics. Hence, the contact forces will always stay current during the iteration. To demonstrate the effectiveness of the approach, two examples involving the interaction of a tire with three types of soil are solved.

## 2. Bekker model

### 2.1. Pressure–sinkage relationship

Fig. 1 depicts a typical pressure–sinkage relationship of the Bekker model. It consists of three paths: the loading path  $OA$  where sinkage  $z$  increases with applied pressure  $p$ ; the unloading path  $AB$  where the soil does

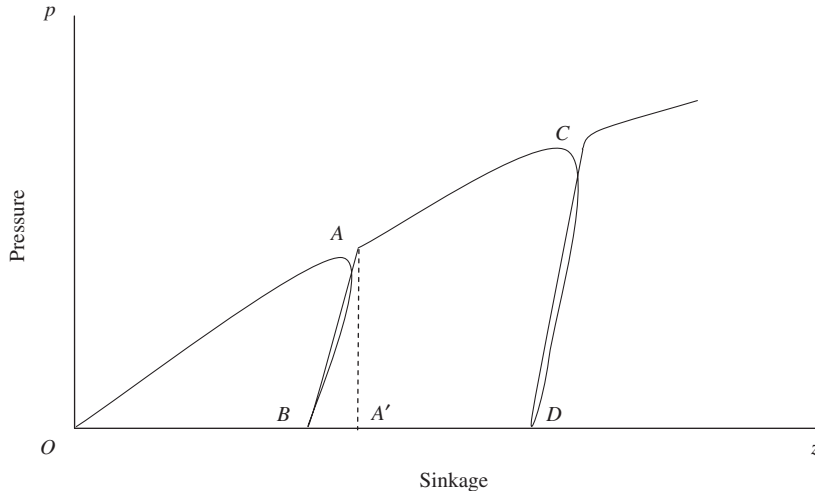


Fig. 1. Loading, unloading and reloading paths of the Bekker model.

not recover completely, giving rise to an irrecoverable or plastic sinkage  $OB$  and a recoverable or elastic sinkage  $BA'$ , and the reloading path  $BA$ . Further plastic sinkage is produced as the system undergoes repetitive reloading and unloading. The Bekker model is in effect, similar to a one-dimensional elastic–plastic model.

To characterize the pressure–sinkage relationship during the loading phase, Bekker [12] proposed the following equation:

$$p = \left( \frac{k_c}{b} + k_\phi \right) z^n, \tag{1}$$

where  $k_c$  is the cohesive soil modulus,  $b$  the smaller dimension of the tire footprint,  $k_\phi$  the friction soil modulus and  $n$  an exponent. These parameters are usually determined empirically. Based on a typical response of a mineral terrain to repetitive loading, Wong and Preston-Thomas [13] have suggested a pressure–sinkage relationship for the unloading–reloading stage:

$$p = p_u - k_u(z_u - z). \tag{2}$$

Note that  $p_u$  and  $z_u$  are, respectively, the pressure and sinkage at the start of the unloading and are related by

$$p_u = k_{eq} z_u^n, \tag{3}$$

in which  $k_{eq} = (k_c/b + k_\phi)$ . In Eq. (2),  $k_u$  is a parameter representing the average slope of the unloading–reloading line  $AB$ , and is dependent on  $z_u$ . Wong [6] gave an approximate relationship

$$k_u = k_0 + A_u z_u. \tag{4}$$

Once again, the parameters  $k_0$  and  $A_u$  are determined experimentally and are listed in Ref. [6] for selected terrain types.

Since the rebound (i.e. recoverable or elastic sinkage)  $z_e$  is given by  $z_e = k_{eq} z_u^n / k_u$ , the rebound ratio  $\eta$  can be computed from

$$\eta = \frac{z_e}{z_u} \times 100\% = \frac{k_{eq} z_u^{n-1}}{k_0 + A_u z_u} \times 100\%. \tag{5}$$

For certain values of  $z_u$ , the computed rebound ratio in Eq. (5) can exceed 100%, which is incorrect. For example, using the parameters for LETE sand [6] in Table 1, we get  $\eta = 292\%$  and  $126\%$  corresponding to  $z_u = 0.01$  and  $0.02$  m, respectively.

It appears that the source of the problem is the inaccurate linear relationship between  $k_0$  and  $z_u$ , as  $z_u$  approaches very small values. To solve the problem, we are suggesting to use the following linear interpolation

Table 1  
Pressure-sinkage and shear strength parameters for various soil types

Terrain type	Loose sand [10]	Soft soil [6]	LETE sand [6]
$n$	1.6	0.8	0.793
$k_c$ (kN/m $^{n+1}$ )	225.14	16.54	102
$k_\phi$ (kN/m $^{n+2}$ )	2216	911.4	5301
$k_0$ (kPa/m)	0 <sup>a</sup>	0	0
$A_u$ (kPa/m $^2$ )	503,000 <sup>a</sup>	86,000	503,000
$c$ (kPa)	0.6903	3.71	0.7
$\phi$ (deg)	31	25.6	27.5
$K$ (cm)	3.81	2.1	1.0

<sup>a</sup>Assumed value.

for very small  $z_u$ ; specifically, for  $z_u \leq z_{u1}$ :

$$\eta = \eta_0 + \left( \frac{\eta_1 - \eta_0}{z_{u1}} \right) z_u, \quad \eta_1 \leq \eta_0 \leq 1, \quad (6)$$

where the upper limit of the interpolation  $\eta_0$  is estimated by setting  $z_u \rightarrow 0$  and the lower limit  $\eta_1$  is given by  $\eta_1 = k_{eq} z_{u1}^{n-1} / (k_0 + A_u z_{u1})$ . If the computed rebound ratio from Eq. (5) exceeds 100% for given values of  $z_u$ , we may choose  $\eta_0 = 1$  as  $z_u \rightarrow 0$ . Further,  $z_{u1}$  can be determined approximately from experimental data or via Eq. (5). For given values of  $z_u$ , the rebound ratio can be computed and thus, allowing  $z_{u1}$  to be determined. Note that for  $z_u \geq z_{u1}$ ,  $\eta$  should still be obtained from Eq. (5).

### 2.2. Shear stress–displacement relationship

Wong and Preston-Thomas [13] found that for certain types of sand, saturated clay, fresh snow and peat and for rubber-sand, rubber-snow, rubber-muskeg mat and rubber-peat shearing, the shear stress–displacement relationship can be described fairly well by the following set of equations.

$$s = s_{\max}(1 - e^{-j/K}), \quad (7)$$

in which the superscript  $j$  represents the shear displacement,  $K$  the shear deformation modulus and  $s_{\max}$  the maximum shear stress, which can be described by the Mohr–Coulomb equation

$$s_{\max} = c + p \tan \phi. \quad (8)$$

In Eq. (8),  $p$ ,  $c$  and  $\phi$  are, respectively, the normal pressure, the cohesion and the angle of shearing resistance.

### 2.3. Soil damping

To account for equivalent rate effects applied during an unloading and reloading stage of a compacted soil, a parameter defining the soil geometric damping is used. McCullough [14] provided the following expression to describe the damping force of the tire  $F_{sd}$  during the unloading and reloading stage:

$$F_{sd} = \begin{cases} -c_g \dot{z}_c & \text{for } \dot{z}_c > 0 \text{ and } F' \geq 0, \\ 0 & \text{otherwise.} \end{cases} \quad (9)$$

In the above equation,  $c_g$  denotes the geometric damping constant that is determined experimentally, and  $\dot{z}_c$  is the vertical velocity of tire. Also term  $F'$  is defined by  $F' = W - c_g \dot{z}_c$ , where  $W$  is the vertical force arising from the normal pressure and shear stress due to the tire–soil interaction as sketched in Fig. 2, and is given by

$$W = b_{tr} R \left\{ \int_0^{\theta_F} [p(\theta) \cos \theta + s(\theta) \sin \theta] d\theta + \int_0^{\theta_B} [p(\theta) \cos \theta - s(\theta) \sin \theta] d\theta \right\}. \quad (10)$$

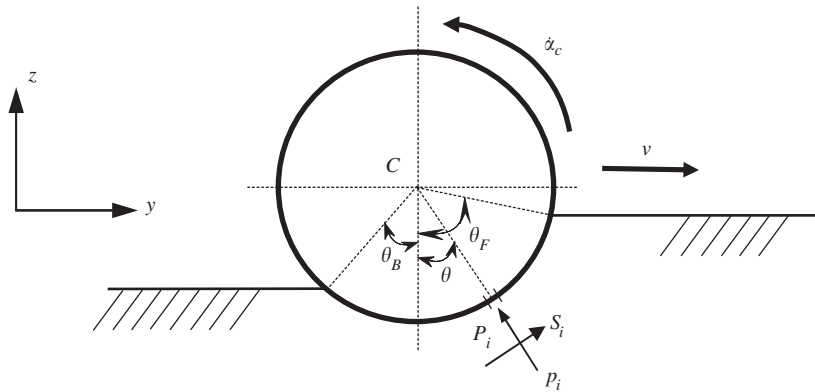


Fig. 2. Tire–soil interaction model.

### 3. The incremental Bekker model

As discussed previously, the pressure on the soil depends on the sinkage, as well as, on the pressure path in reaching the state. To model a tire–soil interaction problem described by the pressure–sinkage relationship given by Eqs. (1) and (2), it is necessary to employ an iterative procedure. This is not only due to the nonlinear relationship between  $z$  and  $p$  in Eq. (1), but also, because a different governing equation is required to describe the loading and unloading status of the soil. In order to reduce the computational complexity, an incremental form is proposed and presented in this section. In the proposed method, the nonlinear relationship between  $z$  and  $p$  is linearized at every incremental step. The loading and unloading status are then described via a set of complementarity equations.

Following the approach in the classical theory of plasticity [15], the pressure function during plastic flow  $f$  can be written as

$$f = p - p_u = 0. \tag{11}$$

The total incremental sinkage from time  $t_0$  to  $t_0 + \Delta t$  can be taken as the sum of the elastic and plastic incremental sinkage. That is,

$$dz = dz_e + dz_p. \tag{12}$$

Eq. (2) can also be expressed in the following alternate form:

$$p = k_u(z - z_p). \tag{13}$$

Differentiating yields the pressure increment

$$dp = k_u(dz - dz_p). \tag{14}$$

The consistency condition  $df = 0$  for the plastic flow must hold and applying it to the total differential of  $f$  leads to

$$df = dp - \frac{dp_u}{dz_p} dz_p = 0. \tag{15}$$

From Eqs. (2) and (5), we have

$$p_u = k_u(z_u - z_p) = (k_0 + A_u z_u)(z_u - z_p), \tag{16}$$

where  $z_u$  can be eliminated via Eq. (3). Differentiating both the sides of Eq. (16) with respect to  $z_p$ , we obtain

$$\frac{dp_u}{dz_p} = \frac{nk_u p_u}{-np_u + A_u(z_u)^2 - A_u z_p z_u + k_u z_u} = k_p, \tag{17}$$

or

$$dp_u = k_p dz_p. \tag{18}$$

When  $z_u \leq z_{u1}$ , we have  $k_p = np_u / [z_u(1 - \eta_0 - 2\eta_1 z_u)]$ .

The governing equations for the incremental Bekker model can thus be summarized into the following compact form:

$$dp = k_u(dz - dz_p), \tag{19}$$

$$(p - p_u)dz_p = 0, \tag{20}$$

$$p - p_u \leq 0, \tag{21}$$

$$dz_p \geq 0. \tag{22}$$

Introducing a non-negative parameter  $v$ , the above equations can be re-written into a set of complementarity equations:

$${}^0p - {}^0p_u + dp - k_p dz_p + v = 0, \tag{23}$$

$$v dz_p = 0, \tag{24}$$

$$dz_p \geq 0, \quad v \geq 0. \tag{25}$$

Note that the left superscript “0” symbolizes quantities at time  $t_0$ , and in subsequent equations, the left superscript “1” denotes them at the incremented time  $t_0 + \Delta t$ . Eqs. (23)–(25) can be regarded as an incremental form of the original Bekker’s pressure–sinkage relationship given by Eqs. (1) and (2). The Lemke algorithm [16,17] can be employed to solve the most general form of the proposed incremental model. However, for some simple cases, such as when  $dp$  is known, the solution can be obtained quite easily.

During unloading, we have  $dp \leq 0$ ,  ${}^0p + dp - {}^0p_u \leq 0$ , and thus,  $dz_p = 0$ . That is,

$$dz = \frac{dp}{k_u}. \tag{26}$$

On the other hand, during loading  $dp \geq 0$  and  ${}^0p + dp - {}^0p_u \geq 0$ , and thus

$$dz_p = \frac{{}^0p + dp - {}^0p_u}{k_p} \quad \text{and} \quad dz = \frac{dp}{k_u} + dz_p. \tag{27}$$

Finally, during reloading  $dp \geq 0$  and  ${}^0p + dp - {}^0p_u \leq 0$ . For this situation, we have

$$dz = \frac{dp}{k_u}. \tag{28}$$

#### 4. Modeling the tire–soil contact

Fig. 2 depicts the model used for the contact analysis between the tire and soil. In the sketch, the contact area of the tire with the soil is discretized into  $m$  segments each of length  $l_s$ , and  $P_i$  which denotes the  $i$ th contact point between the tire and the soil, is assumed to be positioned at the mid-point of the  $i$ th contact segment. The contact forces at  $P_i$  are the normal pressure  $p_i$  and the friction stress  $f_i$  at time  $t_0 + \Delta t$ . Note that  $f_i$  arises due to the soil shear stress  $s_i$  at the coincident contact point located on the soil  $P'_i$ .

Also, let the position of the tire’s mass center be denoted by  $C(y_c, z_c)$ , and the angle of rotation of the tire by  $\alpha_c$ . With these specifications, the equations of motion of the tire can be written as

$${}^1\ddot{y}_c = \frac{F_y}{M} - l_s b_{tr} \sum_{k=1}^m \frac{p_k \sin \theta_k + f_k \cos \theta_k}{M}, \tag{29}$$

$${}^1\ddot{z}_c = \frac{F_z}{M} + l_s b_{tr} \sum_{k=1}^m \frac{p_k \cos \theta_k - f_k \sin \theta_k}{M}, \tag{30}$$

$${}^1\ddot{\alpha}_c = \frac{T_x}{J} - l_s b_{tr} \sum_{k=1}^m \frac{f_k R}{J}, \tag{31}$$

in which  $F_y, F_z$  and  $T_x$  are the applied forces and torque acting on the tire,  $R$  is the radius of tire, and  $M$  and  $J$  are the mass and moment of inertia of the tire, respectively. Integrating Eqs. (29)–(31) yield expressions for velocities and positions, namely,

$${}^1\dot{y}_c = {}^0\dot{y}_c + \frac{1}{2} \left( {}^0\ddot{y}_c + \frac{F_y}{M} \right) \Delta t - \frac{l_s b_{tr}}{2} \sum_{k=1}^m \frac{p_k \sin \theta_k}{M} \Delta t - \frac{l_s b_{tr}}{2} \sum_{k=1}^m \frac{f_k \cos \theta_k}{M} \Delta t, \tag{32}$$

$${}^1\dot{z}_c = {}^0\dot{z}_c + \frac{1}{2} \left( {}^0\ddot{z}_c + \frac{F_z}{M} \right) \Delta t + \frac{l_s b_{tr}}{2} \sum_{k=1}^m \frac{p_k \cos \theta_k}{M} \Delta t - \frac{l_s b_{tr}}{2} \sum_{k=1}^m \frac{f_k \sin \theta_k}{M} \Delta t, \tag{33}$$

$${}^1\dot{\alpha}_c = {}^0\dot{\alpha}_c + \frac{1}{2} \left( {}^0\ddot{\alpha}_c + \frac{T_x}{J} - l_s b_{tr} \sum_{k=1}^m \frac{f_k R}{J} \right) \Delta t, \tag{34}$$

$${}^1y_c = {}^0y_c + {}^0\dot{y}_c \Delta t + \frac{1}{4} \left( {}^0\ddot{y}_c + \frac{F_y}{M} \right) \Delta t^2 - \frac{l_s b_{tr}}{4} \sum_{k=1}^m \frac{p_k \sin \theta_k}{M} \Delta t^2 - \frac{l_s b_{tr}}{4} \sum_{k=1}^m \frac{f_k \cos \theta_k}{M} \Delta t^2, \tag{35}$$

$${}^1z_c = {}^0z_c + {}^0\dot{z}_c \Delta t + \frac{1}{4} \left( {}^0\ddot{z}_c + \frac{F_z}{M} \right) \Delta t^2 + \frac{l_s b_{tr}}{4} \sum_{k=1}^m \frac{p_k \cos \theta_k}{M} \Delta t^2 - \frac{l_s b_{tr}}{4} \sum_{k=1}^m \frac{f_k \sin \theta_k}{M} \Delta t^2, \tag{36}$$

$${}^1\alpha_c = {}^0\alpha_c + {}^0\dot{\alpha}_c \Delta t + \frac{1}{4} \left( {}^0\ddot{\alpha}_c + \frac{T_x}{J} \right) \Delta t^2 - \frac{l_s b_{tr}}{4} \sum_{k=1}^m \frac{f_k R}{J} \Delta t^2. \tag{37}$$

The velocity and position at the contact point on the tire  $P_i$  at time  $t_0 + \Delta t$  are

$${}^1\dot{y}_i = {}^1\dot{y}_c + {}^1\dot{\alpha}_c R \cos \theta_i, \tag{38}$$

$${}^1\dot{z}_i = {}^1\dot{z}_c + {}^1\dot{\alpha}_c R \sin \theta_i, \tag{39}$$

$${}^1y_i = {}^1y_c + R \sin \theta_i, \tag{40}$$

$${}^1z_i = {}^1z_c - R \cos \theta_i. \tag{41}$$

In view of Eqs. (32)–(37), Eqs. (38)–(41) can be compactly re-written as

$${}^1\dot{y}_i = F_{1ik}^n p_k + F_{1ik}^t f_k + \gamma_{1i}, \tag{42}$$

$${}^1\dot{z}_i = F_{2ik}^n p_k + F_{2ik}^t f_k + \gamma_{2i}, \tag{43}$$

$${}^1y_i = T_{1ik}^n p_k + T_{1ik}^t f_k + \pi_{1i}, \tag{44}$$

$${}^1z_i = T_{2ik}^n p_k + T_{2ik}^t f_k + \pi_{2i}, \tag{45}$$

where

$$F_{1ik}^n = -\frac{\sin \theta_k}{2M} l_s b_{tr} \Delta t, \quad F_{1ik}^t = -\left( \frac{\cos \theta_k}{2M} + \frac{R^2 \delta_{ik} \cos \theta_k}{2J} \right) l_s b_{tr} \Delta t,$$

$$\gamma_{1i} = {}^0\dot{x}_c + \frac{1}{2} \left( {}^0\ddot{x}_c + \frac{F_y}{M} \right) \Delta t + {}^0\dot{x}_c R \cos \theta_i + \frac{1}{2} \left( {}^0\ddot{x}_c + \frac{T_x}{J} \right) \Delta t R \cos \theta_i,$$

$$F_{2ik}^n = \frac{\cos \theta_k}{2M} l_s b_{tr} \Delta t, \quad F_{2ik}^t = - \left( \frac{\sin \theta_k}{2M} + \frac{R^2 \delta_{ik} \sin \theta_k}{2J} \right) l_s b_{tr} \Delta t,$$

$$\gamma_{2i} = {}^0\dot{z}_c + \frac{1}{2} \left( {}^0\ddot{z}_c + \frac{F_z}{M} \right) \Delta t + {}^0\dot{x}_c R \sin \theta_i + \frac{1}{2} \left( {}^0\ddot{x}_c + \frac{T_x}{J} \right) \Delta t R \sin \theta_i,$$

$$T_{1ik}^n = - \frac{\sin \theta_k}{4M} l_s b_{tr} \Delta t^2, \quad T_{1ik}^t = - \frac{\cos \theta_k}{4M} l_s b_{tr} \Delta t^2,$$

$$\pi_{1i} = {}^0y_k + {}^0\dot{y}_c \Delta t + \frac{1}{4} \left( {}^0\ddot{y}_c + \frac{F_y}{M} \right) \Delta t^2 + R \sin \theta_i,$$

$$T_{2ik}^n = \frac{\cos \theta_k}{4M} l_s b_{tr} \Delta t^2, \quad T_{1ik}^t = - \frac{\sin \theta_k}{4M} l_s b_{tr} \Delta t^2,$$

$$\pi_{2i} = {}^0z_c + {}^0\dot{z}_c \Delta t + \frac{1}{4} \left( {}^0\ddot{z}_c + \frac{F_z}{M} \right) \Delta t^2 - R \cos \theta_i.$$

### 5. The tire and soil interaction model

To derive the complementarity equations for use in the contact analysis, it is convenient to adopt the following notation; let the contact forces on the tire at  $P_i$ , at the incremented time  $t_0 + \Delta t$  be represented by  $p_i$  and  $f_i$ . Thus, these same forces at the previous time  $t_0$  can be conveniently denoted by  ${}^0p_i$  and  ${}^0f_i$ . From the original set of the complementarity equations given by Eqs. (23)–(25), the sinkage increment from  $t_0$  to  $t_0 + \Delta t$  can be evaluated from the following set of equations:

$$dz_{i'} = \frac{p_i - {}^0p_i}{k_{i'u}} + dz_{i'p}, \tag{46}$$

$$p_i - {}^0p_{i'u} - k_{i'p} dz_{i'p} + \zeta_{i'} = 0, \tag{47}$$

$$\zeta_{i'} dz_{i'p} = 0, \tag{48}$$

$$dz_{i'p} \geq 0, \quad \zeta_{i'} \geq 0. \tag{49}$$

This implies that the sinkage at time  $t_0 + \Delta t$  is  $z_{i'} = {}^0z_{i'} + dz_{i'p}$ . Thus, the  $z$  coordinate of the coincident contact point on the soil  $P'_i$  at time  $t_0 + \Delta t$  can be readily computed and the result is

$$Z_{i'} = \frac{p_i - {}^0p_i}{k_u} + dz_{i'p} + {}^0Z_{i'}. \tag{50}$$

Observe that  ${}^0Z_{i'}$  is the  $z$  of the coincident contact point on the soil  $P'_i$  at time  $t_0$ . From Eqs. (42)–(45) and Eq. (50), the gap function  $g_i^n$  which is defined as the distance from  $P_i$  at the tire to  $P'_i$  at the soil can be readily determined. Likewise, the relative tangential velocity  $\dot{g}_i^t$  can be computed. Their expressions are

$$g_i^n = z_i - Z_{i'} = \bar{T}_{ik}^n p_k + \bar{T}_{ik}^t f_k + dz_{i'p} + \bar{\pi}_i, \tag{51}$$

$$\dot{g}_i^t = \dot{y}_i \cos \theta_i + \dot{z}_i \sin \theta_i = \bar{F}_{ik}^n p_k + \bar{F}_{ik}^t f_k + \bar{\gamma}_i, \tag{52}$$



in which

$$\bar{T}_{ik}^n = T_{2ik}^n + \frac{\delta_{ik}}{K_{iu}}, \quad \bar{T}_{ik}^t = T_{2ik}^t, \quad \bar{\pi}_i = \pi_{2i} - \frac{{}^0p_i}{k_{i'u}} - {}^0Z_i', \quad (53)$$

$$\begin{aligned} \bar{F}_{ik}^n &= F_{1ik}^n \left[ \cos {}^0\theta_i - \left( {}^0\alpha_c - \frac{R\Delta t^2}{4J} \sum_{j=1}^m {}^0f_j \right) \sin {}^0\theta_i \right] \\ &\quad + F_{2ik}^n \left[ \sin {}^0\theta_i + \left( {}^0\alpha_c - \frac{R\Delta t^2}{4J} \sum_{j=1}^m {}^0f_j \right) \cos {}^0\theta_i \right], \end{aligned} \quad (54)$$

$$\begin{aligned} \bar{F}_{ik}^t &= \frac{R\Delta t^2}{4J} F_{1ij}^n {}^0p_j \sin {}^0\theta_i + F_{1ik}^t \left[ \cos {}^0\theta_i - \left( {}^0\alpha_c - \frac{R\Delta t^2}{4J} \sum_{j=1}^m {}^0f_j \right) \sin {}^0\theta_i \right] \\ &\quad + \frac{R\Delta t^2}{4J} \gamma_{1i} \sin {}^0\theta_i - \frac{R\Delta t^2}{4J} F_{2ij}^n {}^0p_j \cos {}^0\theta_i - \frac{R\Delta t^2}{4J} \sum_{j=1}^m {}^0f_j F_{2ik}^t \cos {}^0\theta_i \\ &\quad - \frac{R\Delta t^2}{4J} F_{2ij}^t {}^0f_j \cos {}^0\theta_i + F_{2ik}^t (\sin {}^0\theta_i + {}^0\alpha_c \cos {}^0\theta_i) - \frac{R\Delta t^2}{4J} \gamma_{2i} \cos {}^0\theta_i, \end{aligned} \quad (55)$$

$$\begin{aligned} \bar{\gamma}_i &= -\frac{R\Delta t^2}{4J} \sum_{l=1}^m {}^0f_l F_{1ij}^n {}^0p_j \sin {}^0\theta_i - \frac{R\Delta t^2}{4J} \sum_{l=1}^m {}^0f_l F_{1ij}^t {}^0p_j \sin {}^0\theta_i \\ &\quad + \gamma_{1i} (\cos {}^0\theta_i - {}^0\alpha_c \sin {}^0\theta_i) + \frac{R\Delta t^2}{4J} \sum_{l=1}^m {}^0f_l F_{2ij}^n {}^0p_j \cos {}^0\theta_i \\ &\quad + \frac{R\Delta t^2}{4J} \sum_{l=1}^m {}^0f_l F_{2ij}^t {}^0f_j \cos {}^0\theta_i + \gamma_{2i} (\sin {}^0\theta_i + {}^0\alpha_c \cos {}^0\theta_i). \end{aligned} \quad (56)$$

Summation is not implied by the index  $i$  in all the above equations. For a contact model with friction, the contact conditions include the non-penetration constraint

$$g^n \geq 0, \quad (57)$$

and the friction constraints with a non-negative friction coefficient  $\mu$

$$|f| \leq \mu p, \quad \text{when } \dot{g}^t = 0, \quad (58)$$

$$f = -\text{sign}(\dot{g}^t) \mu p, \quad \text{when } \dot{g}^t \neq 0. \quad (59)$$

Note that the Coulomb friction model is adopted for capturing the dry friction behavior.

Based on the contact conditions given by Eqs. (57)–(59) and noting that  $f_i = \beta_{1i} - \beta_{2i}$  the tire–soil interaction contact model can be compactly described by the following complementarity equations:

$$\psi_i - \bar{T}_{ik}^n p_k - \bar{T}_{ik}^t \beta_{1k} + \bar{T}_{ik}^t \beta_{2k} - dz_{i'p} - \bar{\pi}_i = 0, \quad (60)$$

$$v_{1i} - \zeta_i - \bar{F}_{ik}^n p_k - \bar{F}_{ik}^t \beta_{1k} + \bar{F}_{ik}^t \beta_{2k} - \bar{\gamma}_i = 0, \quad (61)$$

$$v_{2i} - \zeta_i + \bar{F}_{ik}^n p_k + \bar{F}_{ik}^t \beta_{1k} - \bar{F}_{ik}^t \beta_{2k} + \bar{\gamma}_i = 0, \quad (62)$$

$$\eta_i - \lambda(c + p_i \tan \phi)(1 - e^{-j/k}) + \beta_{1i} + \beta_{2i} = 0, \quad (63)$$

$$\zeta_{i'} + p_i - {}^0p_u - k_p dz_{i'p} = 0, \quad (64)$$

$$\psi_i p_i = 0, \quad v_{1i} \beta_{1i} = 0, \quad v_{2i} \beta_{2i} = 0, \quad \eta_i \zeta_i = 0, \quad \zeta_{i'} dz_{i'p} = 0. \quad (65)$$

In the above equations, the quantities  $\psi_i, v_{1i}, v_{2i}, \eta_i, \zeta_i, p_i, \xi_i, \beta_{1i}, \beta_{2i}$ , and  $dz_{i'p}$  are all non-negatives. As before, summing over the index  $i$  in Eq. (65) is not implied. Also, the parameter  $\lambda$  is introduced in Eq. (63) to handle the prescription of soil cohesion (i.e.  $c \neq 0$ ) in the soil model. It takes the following value in accordance to

$$\lambda = \begin{cases} 1 & \text{for } p_i > 0, \text{ i.e. shear stress} = \pm(c + p_i \tan \phi)(1 - e^{-j/k}), \\ 0 & \text{for } p_i = 0, \text{ i.e. shear stress} = 0. \end{cases} \quad (66)$$

Hence, the proposed incremental model consists of the following nonlinear problems: dynamic analysis of the tire as described by Eqs. (29)–(37), and contact interaction analysis between tire and soil and elastic–plastic analysis of the soil as described by Eqs. (60)–(65).

A comparison between the traditional Bekker method and the proposed incremental model is outlined in Table 2. On a cursory glance, they appear to be similar but the incremental approach possesses a distinct advantage over the traditional Bekker method and this difference makes the former to exhibit enhanced computational accuracy and convergency over the latter. As shown in steps 1–2, the two methods solve for the current shear displacement of the soil  $j$  using kinematical quantities of the tire obtained from contact forces: normal pressures and friction stresses computed at the previous iterative approach still relies on contact forces that were determined from the previous iterative step. On the other hand, in the proposed incremental technique, the subsequent tire kinematics were computed using contact forces based on the *current* iterative step (Step 4 in Table 2). This is possible since the pressures and friction forces are obtained simultaneously together with the rest of the tire kinematics during the solution of the set of complementarity equations.

Table 2  
Traditional Bekker method versus incremental Bekker method

Traditional Bekker method	Incremental Bekker method
(1) Compute unknown tire kinematics: $({}^1\dot{y}_c, {}^1\dot{z}_c, {}^1\dot{\alpha}_c)$ and $({}^1\bar{y}_c, {}^1\bar{z}_c, {}^1\bar{\alpha}_c)$ at $t_0 + \Delta t$ from known tire kinematics $({}^0\dot{y}_c, {}^0\dot{z}_c, {}^0\dot{\alpha}_c)$ , $({}^0y_c, {}^0z_c, {}^0\alpha_c)$ at $t_0$ .	(1) Compute unknown tire kinematics: $({}^1\dot{y}_c, {}^1\dot{z}_c, {}^1\dot{\alpha}_c)$ and $({}^1\bar{y}_c, {}^1\bar{z}_c, {}^1\bar{\alpha}_c)$ at $t_0 + \Delta t$ from known tire kinematics $({}^0\dot{y}_c, {}^0\dot{z}_c, {}^0\dot{\alpha}_c)$ , $({}^0y_c, {}^0z_c, {}^0\alpha_c)$ at $t_0$ .
(2) Compute shear displacement $j$ of contact segment $i$ at $t_0 + \Delta t$ based on current tire kinematics: $({}^1\dot{y}_c, {}^1\dot{z}_c, {}^1\dot{\alpha}_c)$ and $({}^1\bar{y}_c, {}^1\bar{z}_c, {}^1\bar{\alpha}_c)$ .	(2) Compute shear displacement $j$ of contact segment $i$ at $t_0 + \Delta t$ based on current tire kinematics: $({}^1\dot{y}_c, {}^1\dot{z}_c, {}^1\dot{\alpha}_c)$ and $({}^1\bar{y}_c, {}^1\bar{z}_c, {}^1\bar{\alpha}_c)$ .
(3) Compute kinematics of contact segment $i$ : $({}^1\dot{y}_i, {}^1\dot{z}_i)$ and $({}^1y_i, {}^1z_i)$ at $t_0 + \Delta t$ based on current tire kinematics $({}^1\dot{y}_c, {}^1\dot{z}_c, {}^1\dot{\alpha}_c)$ and $({}^1\bar{y}_c, {}^1\bar{z}_c, {}^1\bar{\alpha}_c)$ using Eqs. (38)–(41).	(3) Compute $\bar{F}_{ik}^n, \bar{F}_{ik}^f, \bar{T}_{ik}^n, \bar{T}_{ik}^f, \bar{\pi}_i$ and $\bar{\gamma}_i$ from Eqs. (53)–(56).
(4) Check loading/unloading-reloading status of contact segment $i$ at $t_0 + \Delta t$ and compute pressure $p_i$ from either Eq. (1) or (2) based on current $({}^1\dot{y}_i, {}^1\dot{z}_i)$ and $({}^1y_i, {}^1z_i)$ .	(4) Solve complementarity equations (60)–(65) using the results of Step 3 for unknown pressure $p_i$ and friction force $f_i$ .
(5) Compute the relative tangential velocity $\dot{g}_i^t$ from Eq. (52) based on current $({}^1\dot{y}_i, {}^1\dot{z}_i)$ ; and compute $S_i$ (i.e. $f_i$ ) from Eq. (7) based on current $p_i$ and $\dot{g}_i^t$ .	(5) Compute tire accelerations $({}^1\ddot{y}_c, {}^1\ddot{z}_c, {}^1\ddot{\alpha}_c)$ based on current contact forces $(p_i/f_i)$ using Eqs. (29)–(31). Then, integrate via Eqs. (32)–(37) for tire kinematics $({}^1\dot{y}_c, {}^1\dot{z}_c, {}^1\dot{\alpha}_c)$ and $({}^1y_c, {}^1z_c, {}^1\alpha_c)$ .
(6) Compute tire accelerations $({}^1\ddot{y}_c, {}^1\ddot{z}_c, {}^1\ddot{\alpha}_c)$ based on current contact forces $(p_i/f_i)$ using Eqs. (29)–(31). Then, integrate via Eqs. (32)–(37) for tire kinematics $({}^1\dot{y}_c, {}^1\dot{z}_c, {}^1\dot{\alpha}_c)$ and $({}^1y_c, {}^1z_c, {}^1\alpha_c)$ .	(6) If $ {}^1y_c - {}^1\bar{y}_c  \leq \varepsilon$ and $ {}^1z_c - {}^1\bar{z}_c  \leq \varepsilon$ , current iteration has converged and increase time by the next time-step for a new round of iteration by going back to Step 1. Otherwise, the computed tire kinematics $({}^1\dot{y}_c, {}^1\dot{z}_c, {}^1\dot{\alpha}_c)$ , $({}^1y_c, {}^1z_c, {}^1\alpha_c)$ from the previous Step 6 are used as predicted values for the next round of local iteration by going back to Step 2.
(7) If $ {}^1y_c - {}^1\bar{y}_c  \leq \varepsilon$ and $ {}^1z_c - {}^1\bar{z}_c  \leq \varepsilon$ , current iteration has converged and increase time by the next time-step for a new round of iteration by going back to Step 1. Otherwise, the computed tire kinematics $({}^1\dot{y}_c, {}^1\dot{z}_c, {}^1\dot{\alpha}_c)$ , $({}^1y_c, {}^1z_c, {}^1\alpha_c)$ from the previous Step 6 are used as predicted values for the next round of local iteration by going back to Step 2.	

This difference in handling not only results in a greater accuracy but also, in an enhanced numerical convergency of the incremental model over the traditional Bekker approach.

## 6. Numerical examples

The tire performance is dependent on its interactive response to the time varying normal pressure and shear stress distributions at the tire–terrain interface [6,18]. From the horizontal component of these distributions the instantaneous motion resistance and thrust can be easily computed. This information, together with the drawbar pull, which represents the difference of the thrust over motion resistance, can then be employed to describe the tractive performance of an off-road tire. In the following two examples, these and other quantities will be calculated as part of the assessment of the proposed tire–soil model. The first example involves dropping a rigid wheel onto soft soil in an effort to determine the acceleration response of the tire and the resulting sinkage of the soil. The second example investigates a moving tire interacting with three soil types: loose sand, soft soil and LETE sand. The resulting drawbar pull, the normal pressure and shear stress at the tire–soil interface are presented.

### 6.1. Example 1: drop wheel test

A rigid wheel impacting soft soil [14] is sketched in Fig. 3 and it is required to compute the acceleration and position responses. The pressure–sinkage and shear strength parameters of soft soil, which are summarized in Table 1, are taken from Wong [6]. Additionally, the adopted values of the geometric damping constant and the damping ratio corresponding to  $z_u \leq 0.1623$  m are  $c_g = 1000$  N s/m and  $\eta = 10\%$ , respectively. A rigid wheel of similar dimensions to the 280/70R20 tire is selected for the numerical simulation. Therefore, it has the following properties: width  $b_{tr} = 0.282$  m, radius  $R = 0.4545$  m, mass  $M = 32$  kg and moment of inertia  $J = 2.273$  kg m<sup>2</sup>.

As shown in Fig. 3, the bottom of the tire is indicated by  $P_t$  and therefore, the height of the drop onto the soil  $P_s$  is  $P_t P_s$ . Two different initial heights are considered in the simulation:  $P_t P_s = 0$  and  $P_t P_s = 10$  mm. The results for accelerations and positions are plotted in Figs. 4 and 5 respectively. Naturally, the acceleration response and sinkage increases with increasing height of drop. This can be seen in the results of  $P_t P_s = 10$  mm in Figs. 4(b) and 5(b).

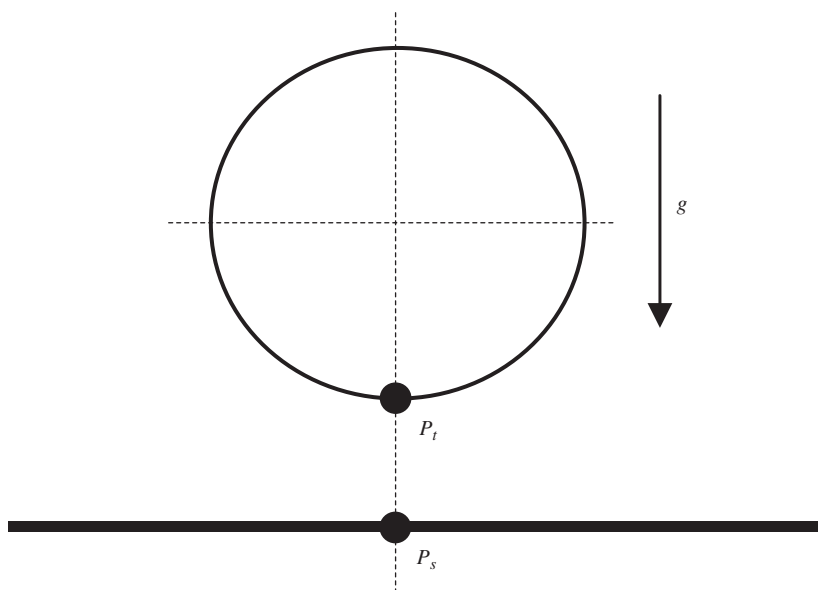


Fig. 3. Rigid wheel dropping on soft soil.

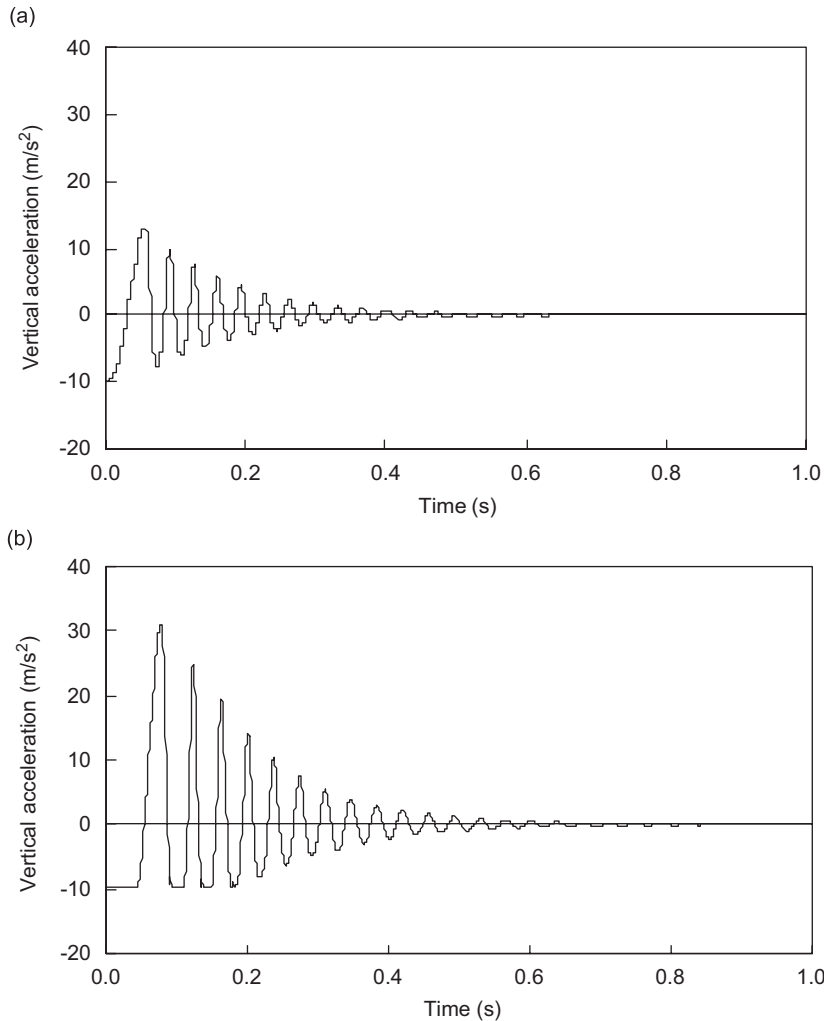


Fig. 4. Vertical acceleration response of tire on soft soil: (a) drop height  $P_t P_s = 0$  and (b) drop height  $P_t P_s = 10$  mm.

In addition, it would be useful to consider the case of zero drop height, i.e.  $P_t P_s = 0$  since a semi-empirical formula for computing sinkage is available for comparison. It is given in Ref. [6] as

$$z_r = \left[ \frac{3W}{b_{tr} \sqrt{2R} (3-n)(k_\phi + k_c/b)} \right]^{2/(2n+1)}, \tag{67}$$

where  $b_{tr}$  is the width of the wheel and  $W$  is the wheel load. Based on the formula, the computed sinkage is 7.2 mm and this figure contrasts reasonably well with the predicted soil sinkage of 7.5 mm based the proposed incremental Bekker model for a tire that has come to a complete standstill. Fig. 6 depicts the variation of sinkage with different drop heights. As shown, the variation for soft soil appears to be leveling off in a linear fashion.

### 6.2. Example 2: moving wheel—modeling tire–soil interaction

This example investigates the interaction of a moving tire with three soil types: loose sand, soft soil and LETE sand. A vertical load (including wheel weight) of 9.28 kN is first applied to the rigid wheel, which is then moved horizontally with prescribed slips. In order to compare the results with Liu and Wong [5] and also, with

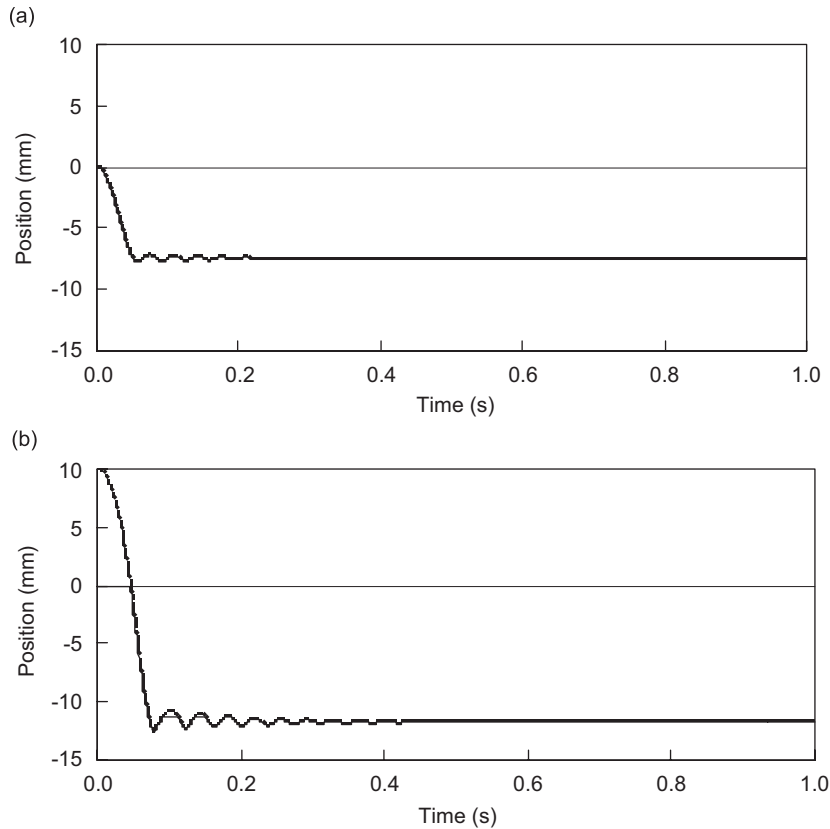


Fig. 5. Vertical positions of the tire on a soft soil: (a) drop height  $P_t P_s = 0$  and (b) drop height  $P_t P_s = 10$  mm, ---  $P_t$  position, —  $P_s$  position.

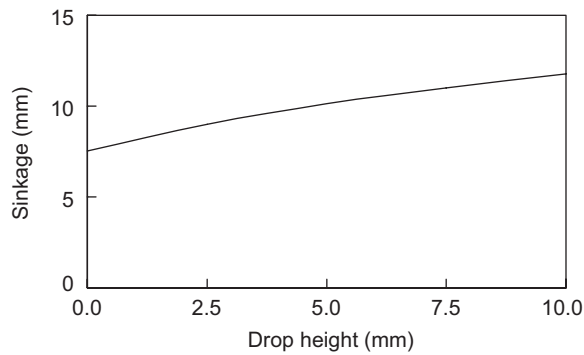


Fig. 6. Variation of sinkage with drop height for tire on soft soil.

Onafeko and Reece [10], we have assumed the rigid wheel to have diameter and width of 1.245 and 0.305 m, respectively. We realized that these are non-standard dimensions but are adopted here to facilitate the comparison. Additionally, the wheel is assumed to have a mass of  $M = 64$  kg, and a moment of inertia of  $J = 4.546$  kgm<sup>2</sup>. The terrain is loose sand as described in Onafeko and Reece [10]. The parameters for pressure–sinkage and shear strength are tabulated in Table 1 under *loose sand*. Since  $k_0$ , and  $A_u$  are not given in either of the two references, we have assumed the following values for them;  $k_0 = 0.0$ ,  $A_u = 503,000$  kN/m<sup>4</sup>. The rebound ratio is taken to be  $\eta = 9.31\%$  for  $z_u \leq 0.001$  m.

Fig. 7 presents the drawbar pull at five prescribed slips of 3.1%, 7.1%, 12.1%, 17.1% and 22.1%. Choosing the two extreme ends of the slips, namely, at 3.1% and 22.1%, the distributions of normal pressure and shear stress along the wheel–sand interface are plotted in Fig. 8(a) and (b), respectively. Superimposed on Fig. 8 for the purpose of comparison are finite element results of Liu and Wong [5], and experimental data of Onafeko and Reece [10].

Observe that the agreement with Onafeko and Reece [10] experimental data is reasonably good, particularly in the trend and pressure magnitudes. However, maximum pressure occurs at the zero angle. This is because in the Bekker approach, the pressure is dependent only on the sinkage (see Eqs. (1)–(3)) and maximum sinkage occurs at the zeroth angle. It should also be pointed out that the  $k_0$  and  $A_u$  values employed in our simulation may be different from those of Refs. [5,6] as they are not listed in the two papers. Further, when  $z_u$  takes on very small values (similar to the one used here), it is necessary to resort to a different equation than the widely accepted linear relationship between  $k_0$  and  $A_u$  for computing the rebound ratio  $\eta$ . We have mentioned in Section 2.1 that the currently used equation is not accurate for very small values of  $z_u$  and we have proposed an alternative equation that we employed to produce our simulation results.

We have also generated similar results for two further terrain types: soft soil and LETE sand. Once again, the parameters for these two soil types are listed in Table 1. For this set of results, a rigid wheel of similar dimensions to the 280/70R20 tire is employed in the simulation with the same physical parameters listed in Example 1. For soft soil, the rebound ratio is taken to be  $\eta = 10\%$  for  $z_u \leq 0.1623$  m and for LETE sand, the corresponding information is  $\eta = 10\%$  for  $z_u \leq 0.1637$  m.

The drawbar pull, and the normal pressure and shear stress distributions along the wheel–sand interface are drawn in Figs. 9–12 for the two selected soils. Figs. 9 and 10 depict the drawbar pull for varying prescribed slips, and Figs. 11 and 12 show the normal pressure and shear stress distributions for the two soil types.

Table 3 lists the sinkage and rebound ratio at varying slips for the three selected soil types. Observe that both sinkage and rebound ratio do not appear to change with the slip.

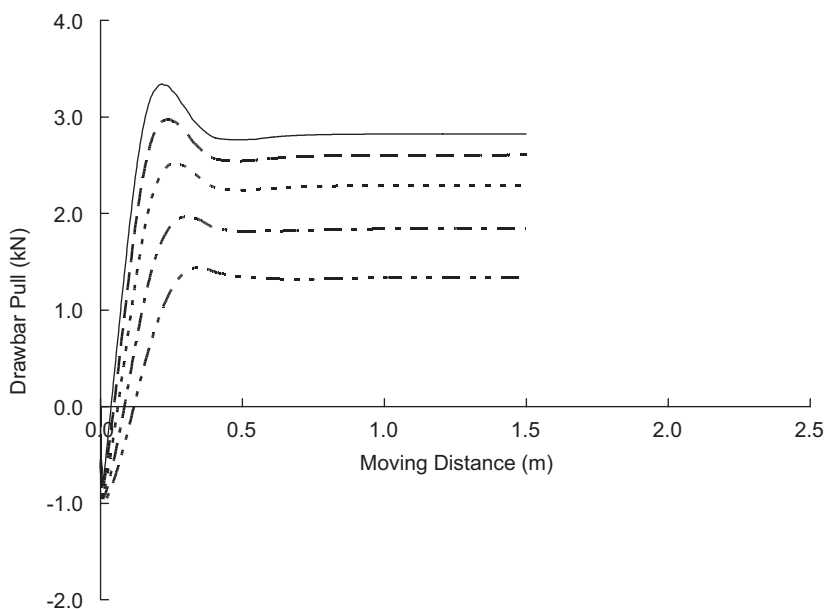


Fig. 7. Drawbar pull of tire on loose sand in a horizontal movement from standstill: — 2.82 at 22.1%, --- 2.60 at 17.1%, ..... 2.29 at 12.1%, - · - 1.84 at 7.1%, - · - · 1.34 at 3.1%.

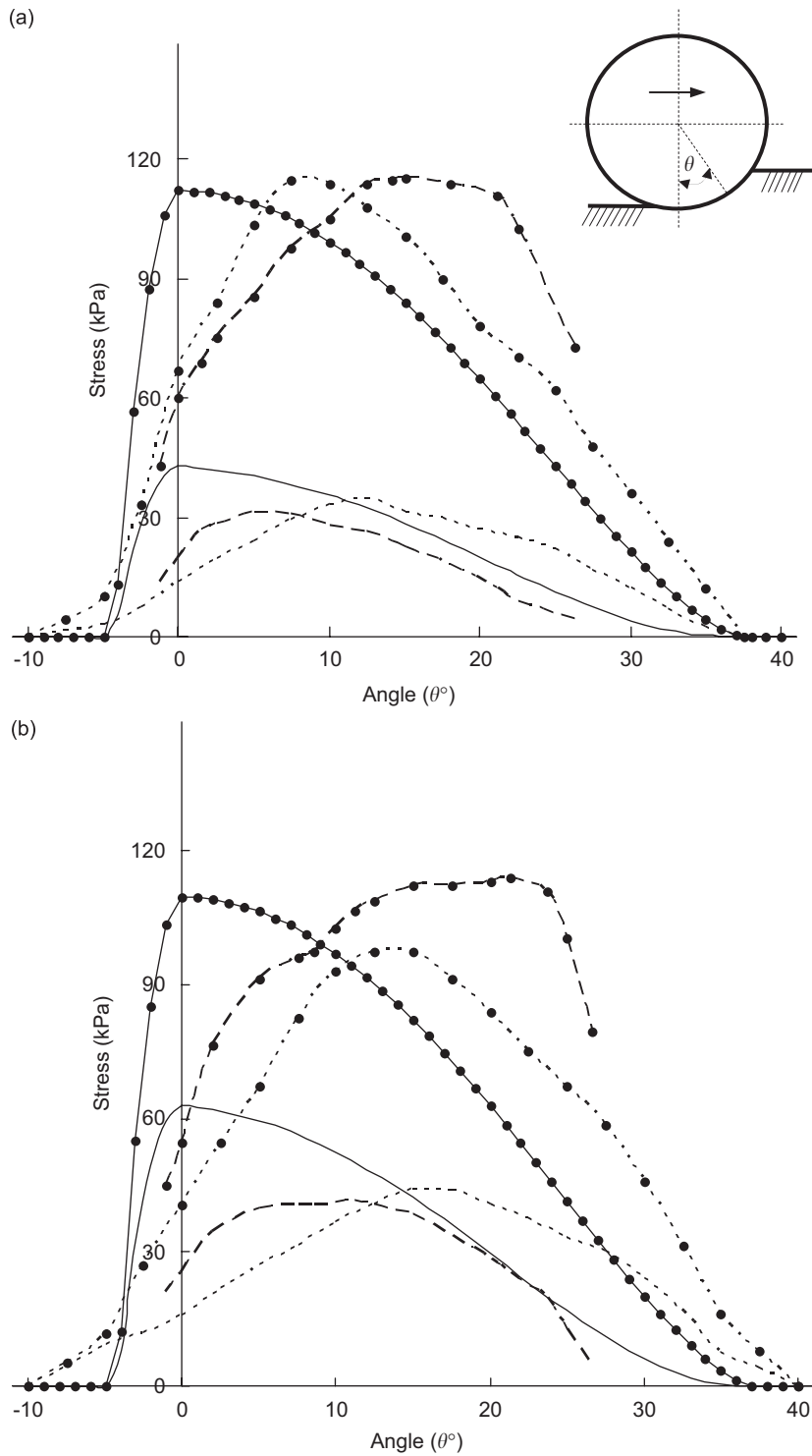


Fig. 8. Normal pressure and shear stress distributions at tire-loose sand interface: (a) 3.1% slip and (b) 22.1% slip, normal pressure (●—● incremental Bekker model, ●—● Liu and Wong [5], ●—● Onafeko and Reece [10]), shear stress (— incremental Bekker model, --- Liu and Wong [5], ..... Onafeko and Reece [10]).

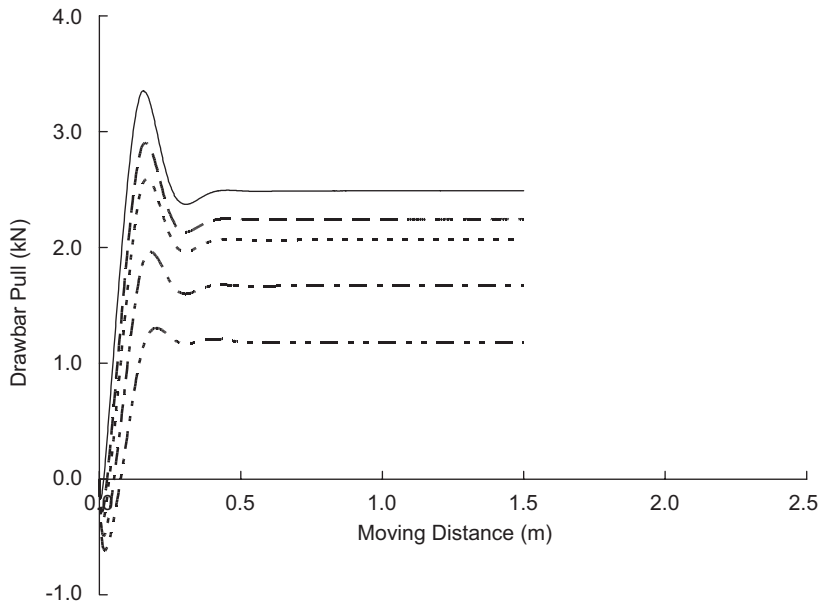


Fig. 9. Drawbar pull of tire on soft soil in horizontal movement from standstill: — 2.49 at 22.1%, --- 2.24 at 17.1%, ..... 2.06 at 12.1%, — · — 1.67 at 7.1%, — · · — 1.18 at 3.1%.

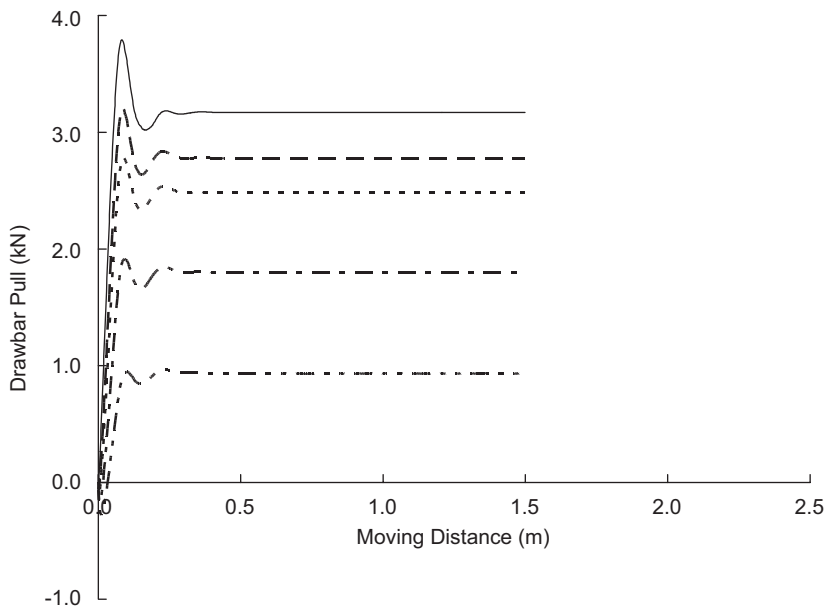


Fig. 10. Drawbar pull of tire on LETE sand in horizontal movement from standstill: — 3.17 at 22.1%, --- 2.78 at 17.1%, ..... 2.48 at 12.1%, - · - 1.80 at 7.1%, - · · - 0.93 at 3.1%.

### 7. Conclusion

In this work, an incremental form of the traditional Bekker model for analyzing tire–soil interaction problems is presented. The method involves formulating the contact dynamics in terms of complementarity equations. This approach allows the contact forces to be evaluated as part of the solution of the unknown



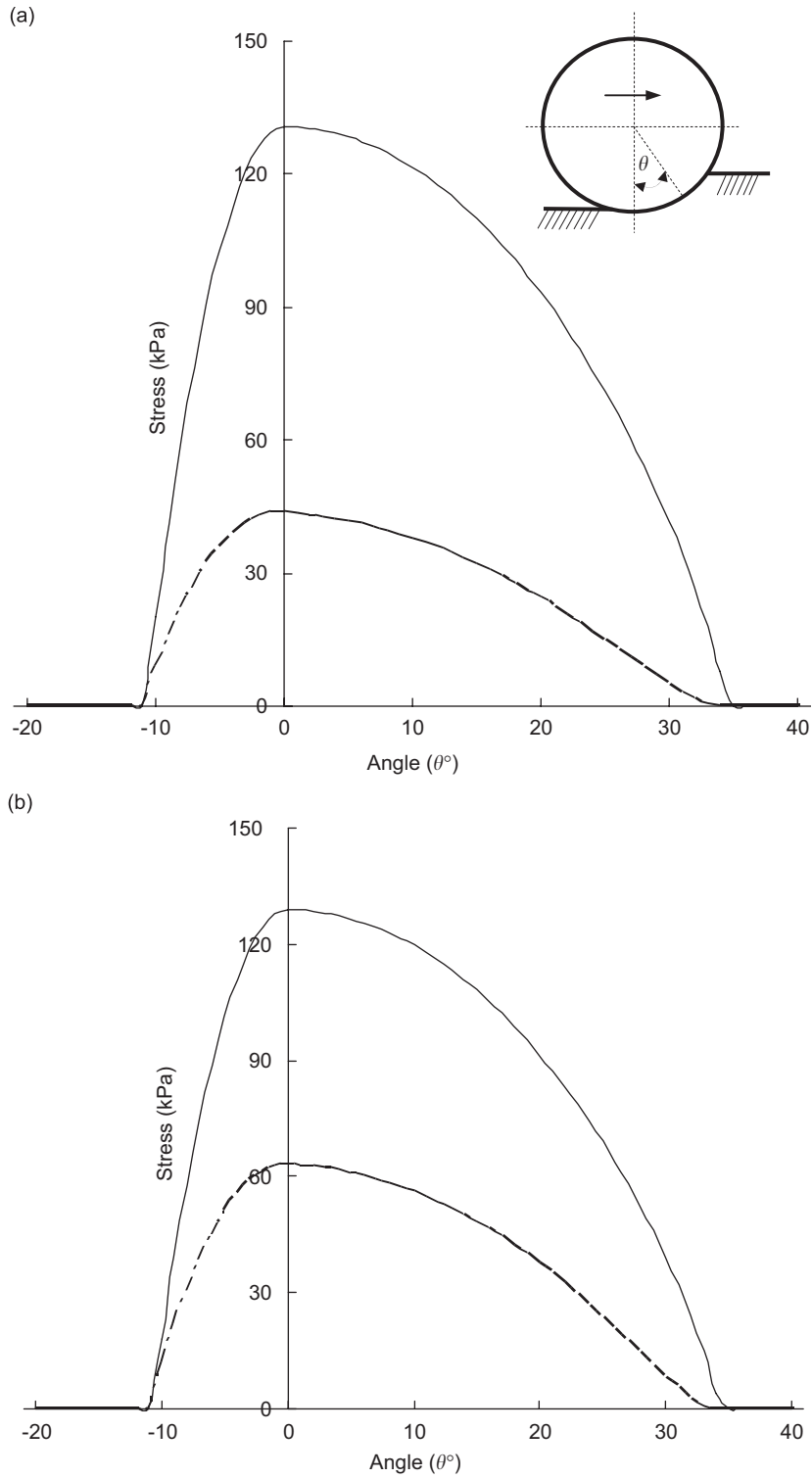


Fig. 11. Normal pressure and shear stress distributions at tire-soft soil interface: (a) 3.1% slip and (b) 22.1% slip, — normal pressure, - - - shear pressure.

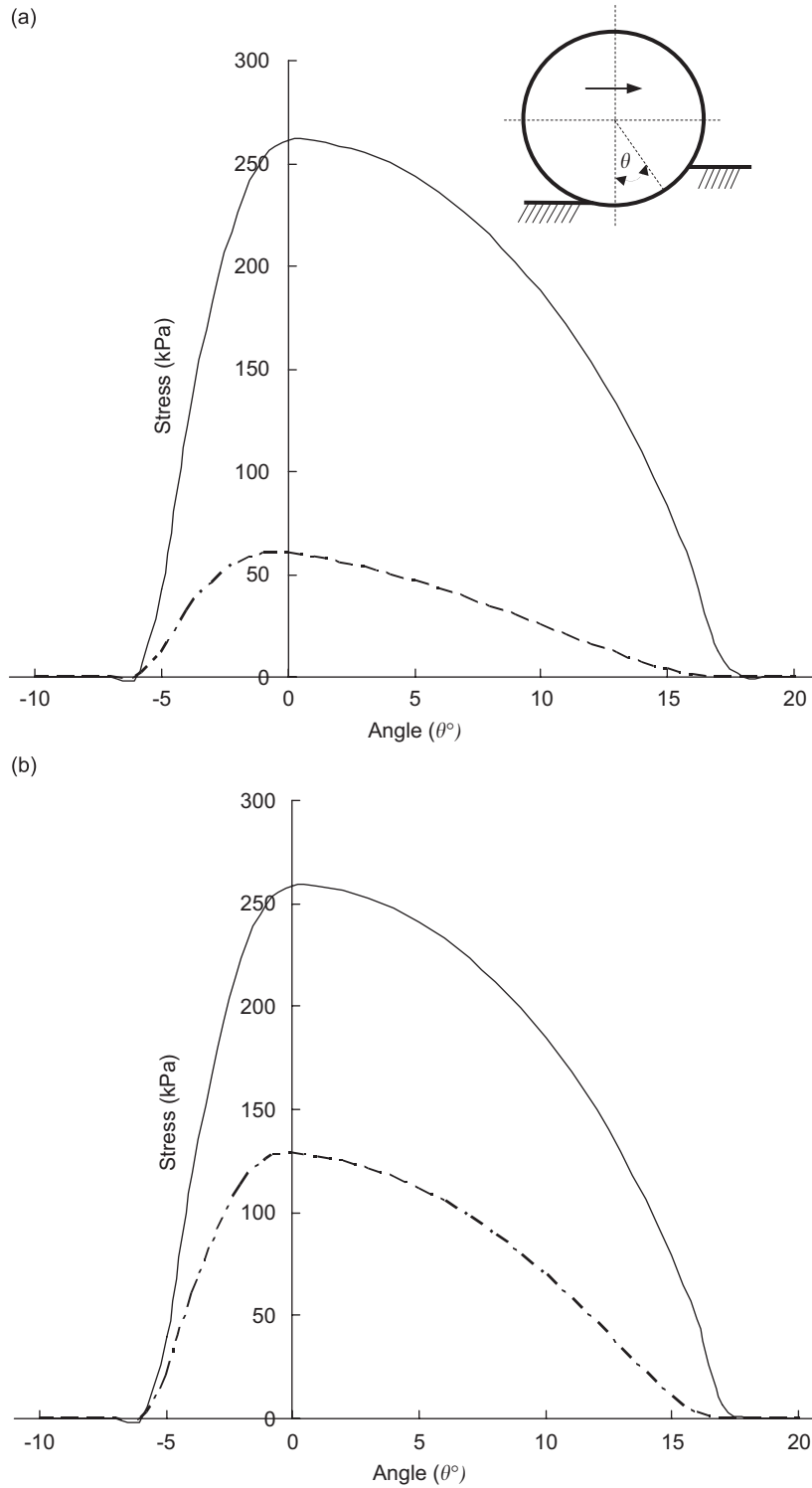


Fig. 12. Normal pressure and shear stress distributions at tire-LETE sand interface: (a) 3.1% slip and (b) 22.1% slip, — normal pressure, - - - shear pressure.

Table 3  
Computed sinkage and rebound ratios for varying slips

Slip (%)	Sinkage (m)			Rebound ratio (%)		
	Loose sand	Soft soil	LETE sand	Loose sand	Soft soil	LETE sand
3.1	0.129	0.080	0.020	1.32	10.19	10.19
7.1	0.129	0.080	0.020	1.33	10.19	10.19
12.1	0.128	0.079	0.020	1.33	10.19	10.19
17.1	0.128	0.079	0.020	1.34	10.19	10.19
22.1	0.128	0.079	0.020	1.33	10.19	10.19

kinematics. Hence, during the iteration the contact forces will always stay current, as opposed to the use of contact forces that have been evaluated at the previous time-step in the traditional Bekker method. The net result is enhanced computational accuracy and convergency of the proposed incremental Bekker approach over the traditional Bekker method. Two examples are described as part of the assessment of the new tire–soil interaction model. Information involving soil sinkage, drawbar pull, and normal pressures and shear stress at the tire–soil interface for three different soil types is provided in comparison with published results. The comparison shows good agreement.

### Acknowledgment

The authors gratefully acknowledge the National Natural Science Foundation of China for providing funding for this work under Grant no. 50475048.

### References

- [1] I.C. Schmid, Interaction of vehicle and terrain results from 10 years research at IKK, *Journal of Terramechanics* 32 (1995) 3–26.
- [2] M.G. Bekker, *Introduction to Terrain-Vehicle Systems*, University of Michigan Press, Ann Arbor, MI, 1969.
- [3] A.A. Rula, C.J. Nuttall, *An analysis of ground mobility models (ANAMOB)*, Technical Report M71-4, U.S. Army Engineer Waterways Experiments Station, Vicksburg, Mississippi, 1971.
- [4] T. Hiroma, S. Wanji, T. Kataoka, Y. Ota, Stress analysis using FEM on stress distribution under a wheel considering friction with adhesion between a wheel and soil, *Journal of Terramechanics* 34 (1997) 225–233.
- [5] C.H. Liu, J.Y. Wong, Numerical simulations of tire–soil interaction based on critical state soil mechanics, *Journal of Terramechanics* 33 (1996) 209–221.
- [6] J.Y. Wong, *Terramechanics and Off-road Vehicle*, Elsevier, Amsterdam, 1989.
- [7] D. Wulfsohn, S.K. Upadhyaya, Prediction of traction and soil compaction using three-dimensional soil-type contact profile, *Journal of Terramechanics* 29 (1992) 541–564.
- [8] F.R. Fassbender, C.W. Fervers, C. Harnisch, Approach to predict the vehicle dynamics on soft soil, *Vehicle System Dynamics Supplement* 27 (1997) 173–188.
- [9] M. Grahm, Prediction of sinkage and rolling resistance for off-the-road vehicle considering penetration velocity, *Journal of Terramechanics* 28 (1991) 339–347.
- [10] O. Onafeko, A.R. Reece, Soil stresses and deformations beneath rigid wheels, *Journal of Terramechanics* 4 (1967) 59–80.
- [11] K.A. Abd El-gawwad, D.A. Crolla, A.M.A. Soliman, F.M. El-Sayed, Off-road tyre modelling I: the multi-spoke tyre model modified to include the effect of straight lugs, *Journal of Terramechanics* 36 (1999) 3–24.
- [12] M.G. Bekker, *Off-the-Road Locomotion*, University of Michigan Press, Ann Arbor, MI, 1960.
- [13] J.Y. Wong, J. Preston-Thomas, On the characterization of shear stress–displacement relationship of terrain, *Journal of Terramechanics* 19 (1983) 107–127.
- [14] M.K. McCullough, *Terra-Dynamics of High Mobility Track Vehicles*, PhD Dissertation, University of Iowa, 1985.
- [15] W.F. Chen, D.J. Han, *Plasticity for Structural Engineers*, Springer, Berlin, 1988.
- [16] J.S. Pan, J.C. Trinkle, Complementarity formulations and existence of solutions of dynamic multi-rigid-body contact problems with Coulomb friction, *Mathematical Programming* 73 (1996) 199–226.
- [17] R.W. Cottle, J.S. Pang, R.E. Stone, *The Linear Complementarity Problem, Series on Computer Science and Scientific Computing*, Academic Press, Boston, 1992.
- [18] J.Y. Wong, M. Garber, J. Preston-Thomas, Theoretical prediction and experimental substantiation of the ground pressure distribution and tractive performance of tracked vehicles, *Proceedings of the Institution of Mechanical Engineers* 198D (1984) 265–285.